Microphase Separation in Model 3-Miktoarm Star Co- and Terpolymers. 2. Dynamics

G. Floudas,*,† N. Hadjichristidis,‡,† H. Iatrou,‡,† and T. Pakula§

Foundation for Research and Technology−Hellas (FO.R.T.H.), Institute of Electronic Structure and Laser, P.O. Box 1527, 711 10 Heraklion Crete, Greece, Department of Chemistry, University of Athens, Panepistimiopolis, Zografou 15771, Athens, Greece, and Max-Planck Institut für Polymerforschung, Postfach 3148, D-55021 Mainz, FRG

Received September 1, 1995; Revised Manuscript Received February 2, 1996[⊗]

ABSTRACT: Dielectric spectroscopy has been employed to study the local and global dynamics of polyisoprene in the asymmetric star (polystyrene)(polyisoprene)$_2$ (SI_2) and in the 3-miktoarm star terpolymer (polystyrene)(polyisoprene)(polybutadiene) (SIB). All measurements refer to the ordered phase where PS cylinders are embedded on the I and I/B matrix, respectively. Effectively, we are studying the local and global dynamics of tethered PI chains in two environments: one made by I-chains (SI_2) and another by the I/B-chains (SIB). At low temperatures, the PI local segmental dynamics in SI_2 and SIB are different, reflecting the modification of the local friction by introducing the faster PB chains in the latter. At higher temperatures, however, this effect diminishes due to the demixing of I and B. To explore the thermodynamic and mobility effects on the global dynamics, we have studied, respectively, a ternary blend composed of PI, PB, and PS and binary blends of SIB and SI_2 with short PB chains. The PI global dynamics in SI_2 and SIB resemble the dynamics of PI stars with additional entanglement effects in the latter.

Introduction

Unlike polymer blends which phase separate on a macroscopic scale, block copolymers undergo a process known as microphase separation from a homogeneous phase to a variety of spatially periodic structures.[1] The morphology in their ordered phase[2,3] is influenced by (i) the value of the product χN, where χ is the interaction parameter ($\sim T^{-1}$) and N is the number of segments, (ii) the composition, and (iii) the macromolecular architecture. The microphase separation transition (MST) or order−disorder transition (ODT) has pronounced effects on the structure, as studied by small-angle neutron (SANS)[4] or X-ray[5] scattering (SAXS), and on the rheological[6] behavior with a transition from a solid-like response, at lower T, to a liquid-like response at higher T. In a recent communication[7] we have reported on the static and kinetic aspects of the ODT in model 3-miktoarm star copolymers and terpolymers using SAXS and rheology. We found that the asymmetric star of the type (polystyrene)(polyisoprene)$_2$ (SI_2) and the 3-miktoarm star terpolymer of the type (polystyrene)(polyisoprene)(polybutadiene) (SIB) formed hexagonally ordered cylindrical microdomains where the PS cylinders are embedded on the I and I/B matrix, respectively. Both stars undergo a transition to the disordered phase at T_{ODT} = 379 K. The order−disorder transition is revealed by sharp discontinuities in the SAXS and rheological response of the system. Furthermore, the kinetics of ordering revealed a kinetically accessible metastable region which was found to be enlarged as compared to linear diblocks.[7]

In the present work we are studying the dynamics of the I-chains in SI_2 and SIB at temperatures below the order−disorder transition temperature (T_{ODT}), where the I- and B-chains are anchored on the cylinders formed by the PS. Following Stockmayer's classification, PI is a type A polymer with nonzero dipole moment components parallel to the chain contour which shows a "normal mode" in the dielectric relaxation spectrum. Dielectric spectroscopy (DS) is a powerful tool in studying the local and global dynamics of systems possessing dipoles perpendicular and parallel to the chain, respectively. The DS on type A chains was pioneered by Stockmayer[8] and studied extensively by Adachi, Kotaka, and co-workers[9] and by Boese and Kremer.[10] The studies above have shown that PI is an ideal type-A polymer mainly due to the high cis content. Furthermore, very monodisperse samples can be prepared via the anionic polymerization technique, and this is the case with the model systems studied here which possess a polydispersity index ($\bar{M}_w/\bar{M}_n$) of less than 1.05. On the other hand, 1,4PB is not a type A chain, and therefore its global motion is dielectrically inert. The strength of its segmental motion is about one-third that of 1,4PI.

Comparing the dynamics of SI_2 and SIB in their ordered phase, we find that the replacement of the I-block in SI_2 by the B-block in SIB—which is not a type A polymer—has pronounced effects on the local and global dynamics of PI. Both systems exhibit many similarities to the dynamics of PI stars, but additional thermodynamic and mobility effects are needed in the latter for a quantitative comparison. To explore these effects, we have prepared binary blends of SI_2 and SIB with short PB chains as well as a ternary blend composed of PI, PB, and PS.

Experimental Section

Samples. The synthesis of the 3-miktoarm star copolymer SI_2 (simple graft) and the star terpolymer SIB has been reported elsewhere.[11] The PS content was 33% w/w for both samples, and the $\bar{M}_w$ (from low-angle laser light scattering in THF at 298 K) were 25.5×10^3 and 24.7×10^3 g/mol for SI_2 and SIB, respectively. The samples had a narrow molecular weight distribution ($\bar{M}_w/\bar{M}_n \leq 1.04$) as determined by size-exclusion chromatography (SEC) and confirmed by membrane osmometry and low-angle laser light scattering.[7] Blends of SI_2 and SIB with PB have been prepared at a 14% w/w (PB) concentration by addition of toluene and subsequent evapora-

† Foundation for Research and Technology−Hellas (FO.R.T.H.), Institute of Electronic Structure and Laser, Crete.
‡ University of Athens.
§ Max-Planck Institut für Polymerforschung, Mainz.
⊗ Abstract published in *Advance ACS Abstracts,* March 15, 1996.

0024-9297/96/2229-3139$12.00/0

Table 1. Characteristics of the 3-Miktoarm Star Copolymer SI_2, 3-Miktoarm Star Terpolymer SIB, the Ternary Blend S/I/B, and Two SI Diblock Copolymers

sample	$\bar{M}_n^{PS} \times 10^{-3}$ [a]	$\bar{M}_n^{PI} \times 10^{-3}$ [a]	$\bar{M}_n^{PB} \times 10^{-3}$ [a]	$\bar{M}_w \times 10^{-3}$ [b]	$\bar{M}_w/\bar{M}_n$ [c]	f_{PS}	T_{ODT} (K)
SI_2	7.6	8.0		25.5	1.03	0.272	379[d]
SIB	7.9	8.2	7.7	24.7	1.04	0.298	379[d]
S/I/B	7.6	6.8	4.0	19		0.37	
SI-115/85	9.2	7.2		17.2	1.05	0.52	410
SI-10	5.3	5.3		10.8	1.02	0.46	

[a] Vapor pressure osmometry (toluene, 323 K). [b] Low-angle laser light scattering (THF, 298 K). [c] Size-exclusion chromatography (THF, 303 K). [d] Reference 7.

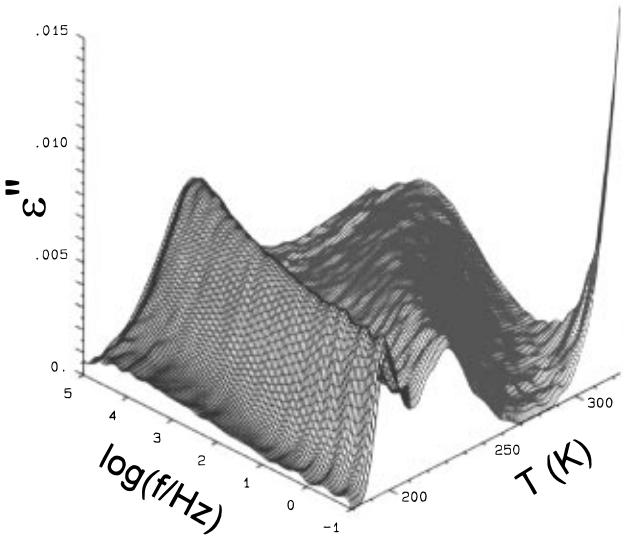

Figure 1. Frequency and temperature dependence of the dielectric loss for SIB showing (i) the "fast" segmental, (ii) the "slow" normal mode, and (iii) the low-frequency conductivity.

tion of the solvent under vacuum for 1 week. The PB sample had the following characteristics: $\bar{M}_n = 960$ (from vapor pressure osmometry), $\bar{M}_w/\bar{M}_n = 1.07$, and microstructure 36% cis-1,4-, 49% trans-1,4-, 15% 1,2-addition. A ternary blend of PS/PI/PB (S/I/B) has been prepared with $w_{PS} = 35\%$ w/w and component molecular weights: $\bar{M}_w^{PS} = 7.6 \times 10^3$, $\bar{M}_w^{PI} = 6.8 \times 10^3$, and $\bar{M}_n^{PB} = 4 \times 10^3$ (PI microstructure: 36% cis-1,4-, 55% trans-1,4-, 9% 1,2-addition). The characteristics of all samples used in the present study are given in Table 1.

DSC. Two glass transition temperatures have been detected (on heating with 10 K/min) in both SI_2 and SIB, corresponding to the isoprene- and styrene-rich phases. The T_g values were 217, 335 K for SI_2 and 204, 338 K for SIB.

Dielectric Spectroscopy (DS). Measurements of the complex dielectric function have been made in the frequency range from 10^{-2} to 10^5 Hz with a frequency response analyzer (Solartron Schlumberger FRA 1260). Additional DS measurements for the ternary blend S/I/B have been made with a Hewlett-Packard HP 4284A impedance analyzer in the frequency rang $20-10^6$ Hz. Measurements were made within the temperature range from 210 to 333 K for SI_2 and from 183 to 363 K for SIB, and therefore, are practically made in their ordered state ($T_{ODT} = 379$ K). The samples were kept between two gold-plated stainless steel plates of 20 mm diameter with a separation of 50 μm. Typical dielectric loss curves for SIB are shown in Figure 1, in a 3-D representation.

Small-Angle X-ray Scattering (SAXS). The SAXS measurements on the bulk SI_2 and SIB have been reported elsewhere.[7] Here we only report the SAXS measurements on the SI_2/B and SIB/B blends. The measurements were made with a Kratky compact camera (Anton Paar KG) equipped with a one-dimensional position sensitive detector (M. Braun), in the temperature range 303−403 K. Details on the SAXS experiment are given in ref 7.

Data Analysis

The complex dielectric permittivity, $\epsilon^*(\omega) = \epsilon'(\omega) - i\epsilon''(\omega)$, of a macroscopic system is given by the Fourier−Laplace transform of the time derivative of the normalized response function $\Phi(t)$ of the polarization $\mathbf{P}(t)$ of the system:

$$\frac{\epsilon^*(\omega) - \epsilon_\infty}{\Delta\epsilon} = \int_0^\infty e^{-i\omega t}\left(-\frac{d\Phi}{dt}\right) dt \qquad (1)$$

where ϵ_0 and ϵ_∞ are the limiting low- and high-frequency permittivities, respectively, and $\Delta\epsilon$ ($=\epsilon_0 - \epsilon_\infty$) is the relaxation strength. $\Phi(t)$ is given by:

$$\Phi(t) = \frac{\langle \mathbf{P}(0)\cdot\mathbf{P}(t)\rangle}{\langle \mathbf{P}(0)\cdot\mathbf{P}(0)\rangle} \qquad (2)$$

and the polarization $\mathbf{P}(t)$ is given by the sum of all dipoles in the system. $\Phi(t)$ can be decomposed into two components: one related to dipole moments $\mu^{\parallel}$ parallel to the chain contour and another to dipole moments $\mu^{\perp}$ perpendicular to the chain contour, thus giving rise to the global normal mode and the local segmental relaxation processes, respectively. In principle, $\mathbf{P}(t)$ contains intra- and intermolecular contributions. Measurements of the dielectric strength as a function of polymer concentration in solutions of cis-PI in a Θ solvent (dioxane) up to the bulk revealed that intermolecular dipole−dipole interactions are negligible.[9c] Furthermore, ignoring the cross terms between the parallel and perpendicular components:

$$\Phi(t) = \frac{\sum_j \sum_m \langle \mu_{ij}^{\parallel}(0)\, \mu_{im}^{\parallel}(t)\rangle + \sum_j \sum_m \langle \mu_{ij}^{\perp}(0)\, \mu_{im}^{\perp}(t)\rangle}{\sum_j \sum_m \langle \mu_{ij}^{\parallel}(0)\, \mu_{im}^{\parallel}(0)\rangle + \sum_j \sum_m \langle \mu_{ij}^{\perp}(0)\, \mu_{im}^{\perp}(0)\rangle} \qquad (3)$$

The parallel component in $\Phi(t)$ corresponds to the end-to-end vector motion:

$$\sum_j \sum_m \langle \mu_{ij}^{\parallel}(0)\, \mu_{im}^{\parallel}(t)\rangle = \mu^2 \langle \mathbf{r}_i(0)\cdot\mathbf{r}_i(t)\rangle \qquad (4)$$

Since the relaxation times of the two components present in $\Phi(t)$ are well separated in the time domain, the individual autocorrelation functions can be calculated. From eqs 1−4 the complex dielectric constant ϵ^* due to the normal mode process is given by:

$$\frac{\epsilon^*(\omega) - \epsilon_\infty}{\Delta\epsilon} = \frac{1}{\langle r^2\rangle}\int_0^\infty e^{-i\omega t}\left[-\frac{d\langle \mathbf{r}(0)\cdot\mathbf{r}(t)\rangle}{dt}\right] dt \qquad (5)$$

where $\langle r^2\rangle$ denotes the mean square end-to-end distance and $\Delta\epsilon$ ($=\epsilon_0 - \epsilon_{\infty,n}$) is the relaxation strength for the normal mode process, with $\epsilon_{\infty,n}$ being the high-frequency limit of the process under investigation.

In the analyses of the DS spectra, we have employed two different approaches. The first is based on the empirical equation of Havriliak and Negmai (HN):

$$\frac{\epsilon^*(\omega) - \epsilon_\infty}{\Delta\epsilon} = \frac{1}{[1 + (i\omega\tau_{HN})^\alpha]^\gamma} \quad (6)$$

where τ_{HN} is the characteristic relaxation time in this equation. The parameters α and γ describe, respectively, the symmetrical and asymmetrical broadening of the distribution of relaxation times. In a log ϵ'' vs log f plot, α and $\alpha\gamma$ give, respectively, the low- and high-frequency slopes of the relaxation function. The two slopes are of particular interest to us since these are affected by long- and short-scale modes, respectively. We will discuss the two slopes later in detail. The rise of $\epsilon''(\omega)$ in Figure 1 at low frequencies is caused by the electrical conductivity of the material, which has been fitted according to $\epsilon'' \sim (\sigma_0/\epsilon_0)\omega^{-1}$, where σ_0 is a fitting parameter and ϵ_0 denotes the permittivity of free space.

The second approach makes no assumption on the form of the relaxation function, and it is based on a transformation of the $\epsilon''(\omega)$ data aiming to obtain the distribution of relaxation times. This approach is based on the inversion of the dielectric data[12]

$$\epsilon''(\omega) = \int_{-\infty}^{+\infty} L(\ln\tau)\frac{\omega\tau}{1 + (\omega\tau)^2}\, d(\ln\tau) \quad (7)$$

using a modified version of CONTIN and provides directly the distribution of relaxation times $L(\ln\tau)$. The result of the inversion of the $\epsilon''(\omega)$ data for the normal modes is shown in Figure 3.

Results and Discussion

Figure 2 compares the dielectric loss of the 3-miktoarm star copolymer SI_2 with that of the star terpolymer SIB at $T \approx 229$ K. At such low temperatures, the segmental process of PI can be clearly resolved, and at lower frequencies there is a contribution from the "slow" normal mode. The separation of the two processes involves both types of analyses (eqs 6 and 7) as a function of temperature. There is a dual structure in both spectra, but the peak related to the local segmental relaxation in SIB is shifted to shorter relaxation times as compared to SI_2. The single segmental relaxation in SIB which is shifted to shorter times implies some degree of mixing of I- and B-chains at low temperatures. This kind of mixing, which probably originates from the closeness of the two T_g's between the two homopolymers ($\Delta T_g = 25$ K), agrees with the single low T_g from DSC. The reverse, that is, a single DSC T_g, does not necessarily imply the existence of a single segmental relaxation. This is known from a variety of "miscible" systems which exhibit a single T_g in DSC, but dynamic experiments have shown two distinct segmental relaxations corresponding to the different relaxing species.[13] This finding also applies to systems where the thermodynamic interactions are switched off ($\chi = 0$).[13g-i]

The miscibility of protonated 1,4PI with protonated 1,4PB (HPI/HPB)[14] and with deuterated 1,4PB (HPI/DPB)[15] have recently been reported. Both systems exhibit a LCST-type phase behavior; that is, they phase separate on heating, in contrast to the expectation borne out by the statistical segment lengths and their T dependence. In the former study,[14] the interaction parameter was calculated on the basis of the mean-field theory and for a 50/50 blend composition was $\chi = (4.68 \times 10^{-3}) - 1.01/T$. The PB microstructure was found to have a pronounced effect on the miscibility of the HPI/HPB blends,[15] and this system is immiscible for less than 24% 1,2PB linkages. In conclusion, the binary

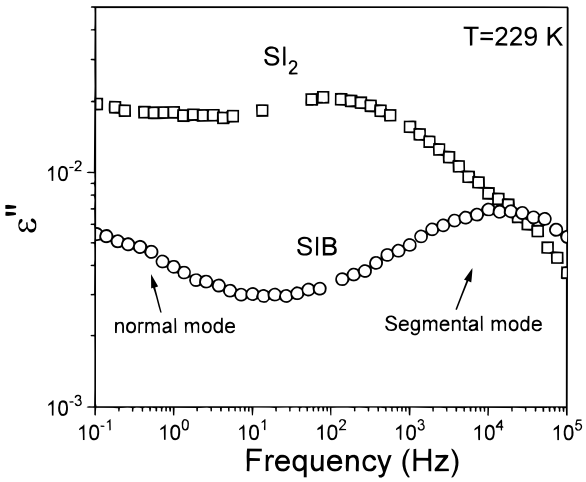

Figure 2. Dielectric loss of the 3-miktoarm star copolymer SI_2 and of the star terpolymer SIB compared at the same temperature $T = 229$ K.

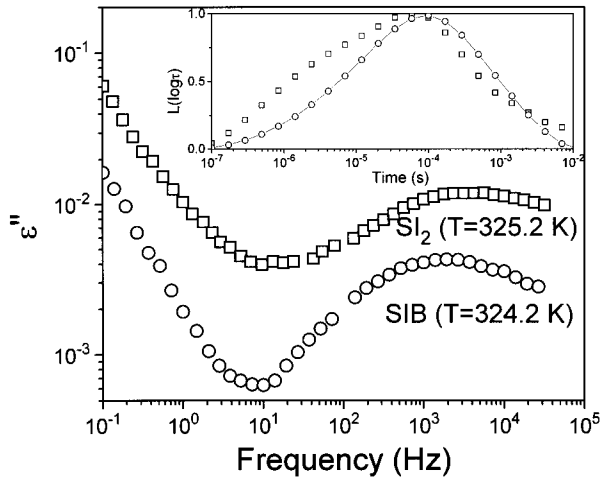

Figure 3. Dielectric loss for SI_2 and SIB at $T = 324$ K as a function of frequency. The corresponding distributions are shown in the inset.

blends of 1,4PB with 1,4PI exhibit a LCST, but the exact location of the phase diagram depends strongly on the 1,2PB content. Our dynamic studies below, which probe heterogeneities on the scale of a few nanometers, provide evidence in support of the LCST-phase behavior in the PI/PB phase of the SIB miktoarm terpolymer and of the S/I/B ternary blend (to be discussed later).

In Figure 3 we plot the dielectric loss of SI_2 and SIB corresponding to the normal mode process. The $\epsilon''(\omega)$ now contains contributions from the conductivity, at low f. The result of the modified CONTIN on the dielectric loss data is shown in the inset. It is worth noticing that the two distributions peak at slightly different times and that the distribution for SI_2 is broader than for SIB.

Before we discuss the temperature dependence of the relaxation times, we first compare the HN distribution parameters for the segmental and normal modes in Figures 4 and 5, respectively. These parameters should be considered with some reserve mainly at low temperatures, since the two distributions overlap. A precise characterization of the broadening for the segmental mode requires the subtraction of the contribution from the normal mode. This is, however, a difficult task without a prior knowledge of the form of the relaxation spectra. Our analysis for the distribution of relaxation times is therefore based on eqs 6 and 7. In Figure 4,

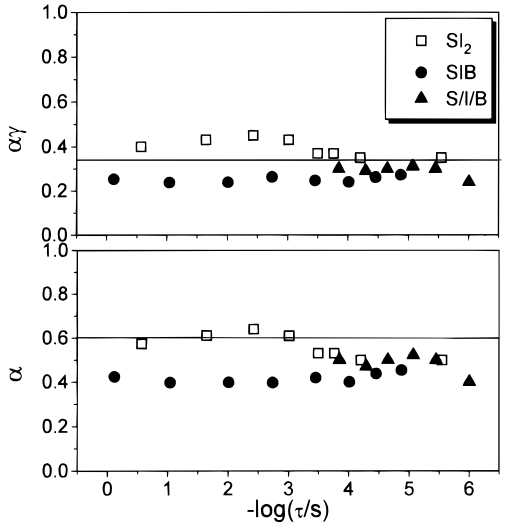

Figure 4. Frequency dependence of the low- (α) and high- ($\alpha\gamma$) frequency slopes corresponding to the segmental mode in SI_2 (□), SIB (●), and the ternary blend S/I/B (▲). The corresponding parameters for the bulk PI are shown by the horizontal lines.

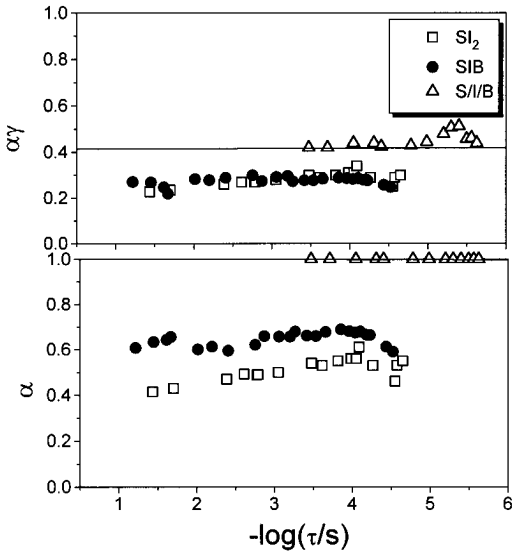

Figure 5. Frequency dependence of the low- (α) and high- ($\alpha\gamma$) frequency limiting slopes corresponding to the normal mode in SI_2 (□), SIB (●), and the ternary blend S/I/B (△). The corresponding parameters for the normal mode of bulk PI with comparable molecular weight are shown by the horizontal lines.

the low- and high-frequency slopes α and $\alpha\gamma$, respectively, are shown for the segmental processes as a function of frequency. The corresponding parameters for bulk PI[10,16]— which are independent of molecular weight—are shown by the solid lines ($\alpha = 0.6$ and $\alpha\gamma = 0.34$). Evidently, the I/B segmental relaxation in SIB is broader when compared to the I-segmental relaxation in SI_2. The latter is indistinguishable from the same parameters in bulk PI. Local concentration fluctuations are responsible for the broadening of the segmental relaxation in SIB in a similar way to polymer blends and block copolymers.[17,13h]

The limiting slopes for the normal mode processes are shown in Figure 5. The corresponding values for the normal mode for a PI-chain[10,16] with a molecular weight comparable to the I-arm in the miktoarms ($\alpha = 1$, $\alpha\gamma = 0.42$) are shown by solid lines. There is considerable broadening of the PI normal mode in the miktoarm stars as compared to bulk PI. This is especially reflected in the low-frequency slopes (α) which assume values of 0.4 and 0.6 for SI_2 and SIB, respectively, instead of $\alpha = 1$ in the bulk PI. This situation here is similar to the weak frequency dependence of G' and G'' observed[5-7] for diblock copolymers below their T_{ODT} which results in the extention of the rubbery plateau and reflects basically a distribution of domain sizes. The broadening of the normal modes in the miktoarms can be discussed separately over the three temperature regimes: (i) at $T > T_{ODT}$, (ii) at $T_g^{PS} < T < T_{ODT}$, and (iii) at $T < T_g^{PS}$. At $T > T_{ODT}$ (disordered phase), the normal mode in a SI copolymer shows the relaxation of the effective dipole moment of the I-block. This relaxation is mainly related to the orientational relaxation of the block which moves relatively freely with the whole chain. The situation becomes drastically different at $T_g^{PS} < T < T_{ODT}$, when the freedom of chains becomes considerably limited by the presence of the interface, especially in the case of the lamellar morphology. The block orientational relaxation is now possible only together with a reorientation of the interface or when the chain escapes from the interface to which it belongs. The two latter effects are considerably slower than the partial relaxation of the block within the microdomain and therefore should lead to a broadening of the normal mode on the low-frequency side. In extremal cases (i.e., when the lateral extension of lamellae is large) even a bifurcation of the normal mode can be expected as a result of the confinement of the chain at the interface, with a fast component related to the block relaxation within the microdomain and a slow component related to a relaxation together with the interface. Both the broadening and the bifurcation of block relaxation have been observed in computer simulated systems of diblock copolymers[18a] and in experiments on symmetric diblocks of styrene and isoprene[18b]. At $T < T_g^{PS}$, the reorientation of the interface and the chain escape is no more possible and the broad normal mode in linear SI diblock copolymers has been attributed[9j] to the *thermodynamic confinement* originating from the balance of the osmotic and elastic requirements for the I-blocks.

It is conceivable that, in polymer blends, this effect should not exist and therefore the normal mode relaxation spectrum should be indistinguishable from the spectrum of bulk PI. To show this, we have prepared a ternary blend of PS/PI/PB (S/I/B) (Table 1) with $f_{PS} = 0.37$ which, as expected, exhibits a single dielectrically active segmental relaxation in the I/B phase together with the PI normal mode. The distribution of relaxation times, parametrized by the HN parameters, is shown by the triangles in Figures 4 and 5 for the segmental and normal modes, respectively. The segmental relaxation in the ternary blend (Figure 4) displays a broadening which is intermediate between the corresponding processes in SIB and SI_2. For the normal mode, however, the HN parameters are $\alpha = 1$ and $\alpha\gamma = 0.45$, which are exactly the values for the normal mode of bulk PI.

The nominal relaxation times, obtained from the fits to eq 6 for the segmental and normal mode processes, are plotted in Figure 6 for SI_2 and SIB, in the usual Arrhenius representation. All the relaxation times in Figure 6 refer to the ordered phase, where PS cylinders are embedded in the I (SI_2) or the I/B (SIB) matrix. A pertinent feature of the relaxation times shown in Figure 6 is that the large difference in the segmental modes between SI_2 and SIB at low T does not find its counterpart in the normal modes at higher T. The latter

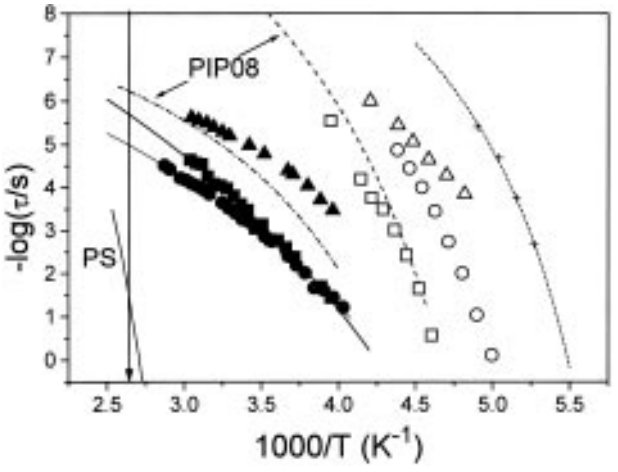

Figure 6. Temperature dependence of the segmental (open symbols) and normal mode (filled symbols) processes in SIB (○), in SI_2 (□), and in the ternary blend S/I/B (△). The segmental relaxations in bulk PB and PI are also shown by the dashed lines (short and long, respectively), and the corresponding normal mode to the PI chain is shown by the dash−dotted line. The vertical line separates the disordered phase at high temperatures from the ordered phase at lower temperatures.

seem to be insensitive to the faster local segmental modes in SIB. We should keep in mind, however, that the two processes are measured in different T ranges. Solid lines in Figure 6 are fits to the Vogel−Fulcher−Tammann (VFT) equation:

$$\log \tau = \log \tau_0 + \frac{B}{T - T_0} \tag{8}$$

where $\log \tau_0$, B, and T_0 are the high-T intercept, the activation energy, and the "ideal" glass transition in this representation. These parameters assume the following values: $\log \tau_0 = -12.25$, $B = 600$ K, and $T_0 = 165$ K for the segmental and $\log \tau_0 = -10.1$, $B = 1113$ K, and $T_0 = 125$ K for the normal mode of SI_2. The segmental relaxation times for the I relaxation in SI_2 are in good agreement with the corresponding times in bulk PI. The normal mode, however, is retarded by nearly one decade, and this is expected for a tethered I-chain since $\tau^{tet} \approx 4\tau^{free}$.[9j,19] It has been discussed in the literature[16] that an extrapolation of the segmental and normal mode processes will result in the crossing of the two—provided that such extrapolation is meaningful— at the same temperature (T_0). This has been discussed in terms of the breakdown of thermorheological simplicity in the vicinity of the crossing temperature.

In Figure 6, we include the segmental (open triangles) and normal mode (filled triangles) processes of the ternary blend S/I/B. With increasing T, the latter relaxation times tend to approach the corresponding modes in the bulk PI. At the same time, the single segmental mode shows a steeper T dependence and at high T approaches the bulk-PI segmental process. This finding indicates a phase transition from a homogeneous I/B phase, at low T, to a phase separated state at high T. Judging from the closeness of the normal mode relaxation time at high T to the corresponding time for the bulk PI, we postulate that the transition, for the blend, occurs at about 300 K. We cannot provide, however, such an estimate for the I/B phase in SIB since the parallel T dependence of the normal modes in SI_2 and SIB indicates a broad range of temperatures where demixing occur.

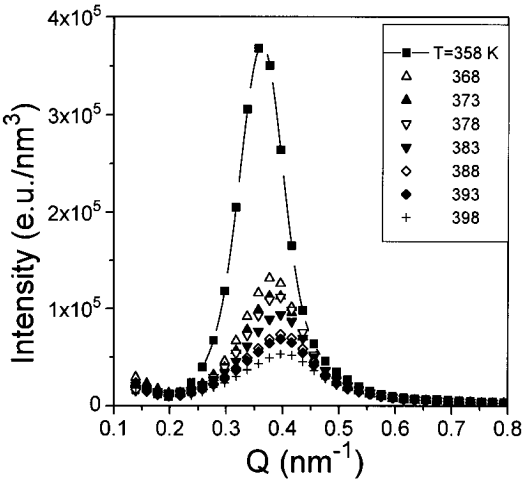

Figure 7. SAXS intensity profiles for the blend SIB/B at different temperatures as indicated. The abropt drop of the peak intensity at $T \approx 360$ K signifies the order−disorder transition.

In the free-draining model proposed by Rouse[20] the correlation function $\langle \mathbf{r}(0)\cdot\mathbf{r}(t)\rangle$ for the normal mode is given by:

$$\langle \mathbf{r}(0)\cdot\mathbf{r}(t)\rangle = \frac{8\langle r^2\rangle}{\pi^2}\sum_p \frac{1}{p^2} e^{-t/\tau_p} \tag{9}$$

and

$$\tau_p = \frac{\zeta N^2 b^2}{3\pi^2 k_B T p^2} \qquad (p\text{: odd}) \tag{10}$$

where τ_p is the relaxation time for the pth mode, b is the average length between beads, and ζ is the friction coefficient per bead, which effectively accounts for the temperature dependence of the relaxation times. In order to further explore the relation between the local friction coefficient and the normal mode relaxation time, we have deliberately changed ζ by introducing short PB chains into SI_2 and SIB. Therefore, two blends have been prepared with a PB of $\bar{M}_w = 960$ at composition $w_{PB} = 14\%$.

Before we realize the comparison of the dynamics in the bulk and diluted (with PB) stars, we should comment on the phase state of the SI_2/B and SIB/B blends, since such a comparison is meaningful only for systems exhibiting the same phase state (ordered phase, in this case). For this purpose, we performed SAXS on the blends, and the desmeared intensity profiles for the system SIB/B are shown in Figure 7 for different temperatures. In both systems there is a discontinuous change of the peak parameters (peak position, width, and intensity) at about 360 K which signifies that the transition temperature from the ordered to the disordered phase has been reduced by about 20 K as compared to the bulk polymers. Therefore, all DS measurements are made within the ordered phase where the styrene cylinders are embedded in the matrix formed by the I/B blocks and the short B-chains.

The two dielectrically active modes in the blends have been fitted with the empirical HN equation (eq 6), and the nominal relaxation times for the blends SIB/B are shown in Figure 8, together with the times for the bulk SIB. The segmental relaxation times of bulk PB[13a] and PI[10b] and the normal mode times of the corresponding

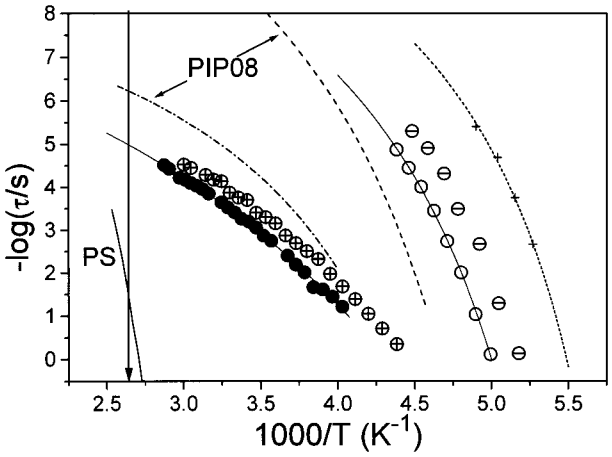

Figure 8. Comparison of the segmental (○) and normal (●) mode relaxation times of SIB with the same processes in the blend SIB/B: (⊖) and (⊕), respectively. The segmental relaxations in bulk PB and PI are also shown by the dashed lines (short and long, respectively), and the corresponding normal mode to the PI chain is shown by the dash−dotted line.

linear PI chain ($\bar{M}_w \approx 8 \times 10^3$) are also plotted in Figure 8. The segmental and normal mode times of the SIB/B blend are clearly modified by the presence of the short B-chains, however, to a different extent. The segmental mode in SIB/B becomes appreciably faster from the corresponding mode in SIB, but there is only a small effect on the normal mode of SIB/B as compared to SIB, at higher T. It seems that the normal modes depend only moderately on the local friction. This again supports a LCST in the I/B system as with the S/I/B blend.

An alternative way of looking into the data is provided by the coupling model.[21] The effect of blending SIB and SI_2 with short PB chains can be likened to the addition of diluent. Previous experience[22] from polymer/additive systems has shown that, at any fixed T, the segmental relaxation time shifts to shorter times more with the addition of diluent than the Rouse modes. This is reflected in the shift factor for the segmental mode a_S being much larger than the corresponding factor for the Rouse mode, i.e., $a_S \gg a_R$. The same reasoning, applies to the comparison between the bulk systems, if we envision SIB as the plasticized version of SI_2 (Figure 6).

The molecular weight dependence of the average relaxation times for the normal modes is shown in Figure 9. The average relaxation times are obtained from $\langle\tau\rangle = (\tau_0/\beta)\Gamma(1/\beta)$, where τ_0 is the nominal relaxation time, β is the Kohlrausch−Williams−Watts parameter for the distribution of relaxation times, and Γ is the gamma function. The procedure used to extract β from the HN parameters α and γ is described elsewhere in detail.[10] The solid line gives the molecular weight dependence of the normal mode relaxation times for linear cis-PI's.[10b] For molecular weights below the critical molecular weight M_c ($\approx 10^4$) the normal mode relaxation time is proportional to M^2, in good agreement with the predictions of eq 10, but at $M \geq M_c$ the slope of the solid line is 3.7 ± 0.3, which is much too high compared to the theoretical prediction for entangled linear chains:[23,24]

$$\langle \mathbf{r}(0)\cdot\mathbf{r}(t)\rangle = \frac{8\langle r^2\rangle}{\pi^2}\sum_p \frac{1}{p^2} e^{-p^2 t/\tau_d} \quad \text{(p: odd)} \qquad (11)$$

and

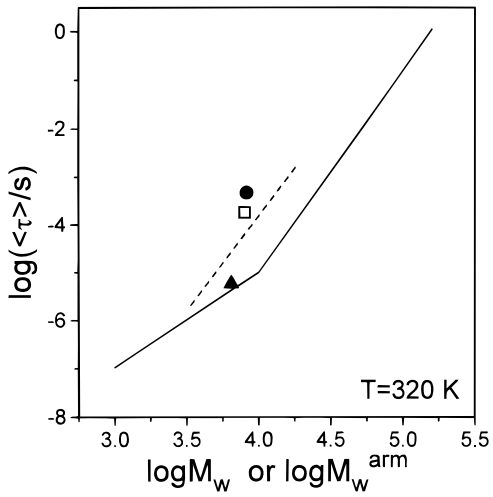

Figure 9. Average relaxation times for the PI normal mode in SI_2 (□), SIB (●), and the ternary blend S/I/B (▲) at $T = 320$ K plotted against the arm molecular weight. The figure includes the molecular weight dependence of the average relaxation times of linear cis-PI (solid line) and of star-shaped PI's (dashed line).

$$\tau_d = \frac{\zeta N^3 b^4}{\pi^2 k_B T d^2} \qquad (12)$$

In eq 12, τ_d is the relaxation time of the first mode (longest relaxation time) and d is the tube diameter. Contour length fluctuations[25] and constraint release effects[26,19] have been proposed to account for the higher exponent. As expected, the average relaxation time for the PI normal mode in the ternary blend S/I/B lies on top of the solid line for the linear cis-PI's. At the same temperature, however, the normal mode average relaxation time for SI_2 and SIB are substantially longer. The dashed line gives the dependence of the relaxation times on the arm molecular weight for PI stars. The latter times were found to be independent of the number of arms and $\tau_{star}/\tau_{linear} = 4.0$.[10a,19] Therefore, the normal mode relaxation time of PI in the SI_2 agrees with that of, i.e., a 3-arm PI star. Interestingly, it is the same factor which appears for tethered chains, i.e., $\tau^{tet} = 4\tau^{free}$.[9j,19] The PI normal mode time in SIB is also plotted in Figure 9 and is somewhat slower, when compared to SI_2, notwithstanding the similar MW of the PI arm (Table 1).

We emphasize this point by comparing the PI normal mode distributions in different environments, at $T = 320$ K in Figure 10. Among the five distributions shown, the narrower—with a low frequency slope of 1—corresponds to the PI in the S/I/B. The broader distribution belongs to a linear and symmetric SI diblock copolymer with $\bar{M}_w = 16\,400$ (Table 1). The T_{ODT} for this sample is 410 K, and below this temperature a lamellar microstructure forms with a domain thickness of about 14 nm. The second broader distribution is for another SI (SI-10) diblock copolymr with $\bar{M}_w = 10\,800$ and a PS volume fraction of $f_{PS} = 0.46$. This diblock when examined by SAXS and rheology exhibits a liquid-like structure with no apparent transition to an ordered phase. The two star systems SI_2 and SIB fall in between, with the former having a slightly broader distribution. It is interesting, at this point, to compare the normalized distributions shown in Figure 10 with the literature data from other SI diblock copolymers and SI/SB diblock copolymer blends. Symmetric SI diblock copolymers in their ordered phase

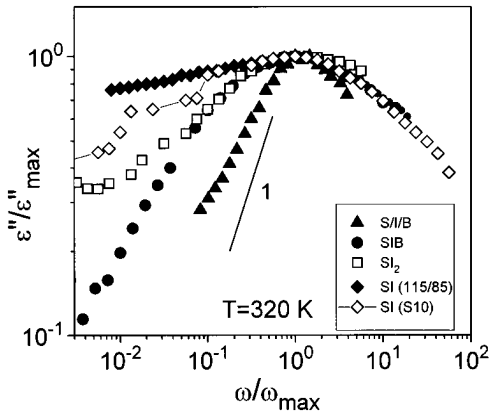

Figure 10. Normalized dielectric loss for the normal mode process in SI_2 (□), SIB (●), and the ternary blend S/I/B (▲). The dielectric loss from two symmetric SI diblock copolymers is also shown: (◇) M_w = 10 800 (disordered state), (♦) M_w = 16 400 (ordered state).

exhibit a broad distribution which can be parametrized as $\alpha \approx {}^1/_4 - {}^1/_3$.[9j,27] However, even the symmetric but homogeneous SI-10 diblock displays a broad distribution ($\alpha \approx {}^1/_3$) which is broader than that for SI_2. The normal mode distribution in SIB ($\alpha \approx {}^2/_3$) can be compared with that in the binary blend SI/SB[9j] which was found to form a lamellar structure with alternating styrene and I/B phases. For the latter system $\alpha \approx 1/4$ and is independent of SI content. Therefore, anchored PI chains on the PS cylinders have a narrower normal mode distribution as compared to the PI normal mode in ordered SI and SI/SB systems forming a lamellar structure. It is not clear, however, whether the narrower distribution in SI_2 and SIB is a result of the different morphology (hexagonal vs lamellar), or of the increased crowding of chains on the PS cylinders.

In the next section we will try to account for the difference in the normal mode dynamics in the two miktoarms. The approach is based on reptation arguments for entangled star-shaped chains. The theoretical work by de Gennes,[28] Doi and Kuzuu,[29] and Pearson and Helfand[30] as well as computer simulations on the dynamics of star molecules[31] revealed a dramatic increase of the viscosity with the molecular weight of the arms:

$$\eta_0 \approx (M_a/M_e)^{1/2} \exp(\nu M_a/M_e) \qquad (13)$$

where η_0 is the zero-shear viscosity, M_e is the molecular weight between entanglements, and ν is a constant assuming a value of about 0.6. For $M_a \gg M_e$, this results in the quenching of the star dynamics since the longest relaxation time of the fluctuation of the branch point-to-end vector of an arm increases proportionately to $\exp(\nu M_a/M_e)$. The longest relaxation time τ_{max} of the fluctuation of the branch point-to-end vector of an arm is given by:[29]

$$\tau_{max} \approx \exp(\nu M_a/M_e) \qquad (14)$$

The longest relaxation time in star polymers can be obtained in rheology from the crossing of the storage and loss moduli, and this time differs from the time corresponding to the G'' (and ϵ'') maximum.[32] Furthermore, the rheological response of block copolymers in their ordered phase ($T \leq T_{ODT}$) is very complex, and the loss moduli in both SI_2 and SIB exhibit a weak frequency dependence[7] ($G'' \approx \omega^{0.33}$) similar to that of ϵ''-

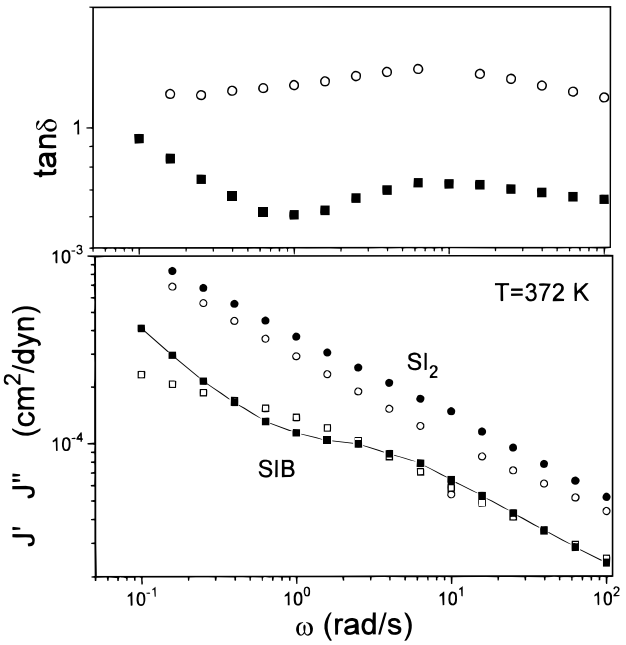

Figure 11. Storage (J') and loss (J'') compliance for SI_2 (circles) and SIB (squares) as a function of frequency at 372 K ($T_{ODT} - T = 7$ K). The broad maximum in the J'' of SIB is absent in SI_2.

(ω) ($\approx\omega^{0.37}$ and $\approx\omega^{0.33}$ for SIB and SI_2, respectively). Nevertheless, for our comparison of the dielectric times, we are using the average relaxation times $\langle\tau\rangle$. Notice that the $\langle\tau\rangle$ can be substantially different from the longest relaxation time τ_{max}, but the former serves for the comparison between the two miktoarm stars (Figure 9). The comparison between the miktoarm stars and linear PI's is only qualitative since the average relaxation time is faster than the long-time edge of the distribution. The calculation of the normal mode retardation in SIB requires knowledge of M_e in the I/B phase. It has been argued[33] that for entangled blends the correct scaling is given by the following rule:

$$\frac{1}{M_e^{1/2}} = \frac{\phi_{PB}}{M_{e,PB}^{1/2}} + \frac{\phi_{PI}}{M_{e,PI}^{1/2}} \qquad (15)$$

Equation 15 predicts a weaker modulus ($G_e \approx M_e^{-1}$) than the one estimated by the linear averaging. Using $\phi_{PI} = \phi_{PB} = 0.5$ and 1900 and 6300 for the molecular weight between entanglements of 1,4PB and 1,4PI, respectively, we obtain $M_e = 3200$. Using eq 14 and the PI-arm molecular weight of Table 1 for SI_2 and SIB, respectively, we obtain the important result that the logarithmic difference between the two normal mode times is 0.4, which is in good agreement with the experimental results of Figure 9. Therefore, although the I-chains in SI_2 are not entangled, the replacement of an I-arm by PB results in the increase of entanglements. Such entanglement constraints are responsible for the positive deviations shown on Figure 9 for the SIB normal mode dynamics. This is supported by measurements of the compliance at a temperature T = 372 K, which is only 7 K below the order−disorder transition temperature. At this temperature, the rheological behavior of both systems shows a non-Newtonian response which practically extends the rubbery plateau to lower frequencies. The result is shown in Figure 11, where we plot the storage (J') and loss (J'') compliance for SI_2 and SIB. The loss compliance in the latter

system displays a broad maximum whose frequency corresponds to the low-frequency end of the extended plateau in the storage modulus. This maximum is absent from SI_2 in agreement with the absence of entanglement effects in this system.

Conclusion

We have studied, for the first time, the local and global dynamics of tethered PI chains in a model miktoarm star copolymer (SI_2) and a star terpolymer (SIB) using dielectric spectroscopy. The pertinent feature of the dynamics of such complex star systems is that the large difference in the PI local segmental modes, at low T, is absent from the normal modes, at higher T. The latter are nearly insensitive to the faster local segmental modes in SIB. This difference can be understood in terms of thermodynamic and mobility effects. The PI global dynamics in SI_2 have similarities to the dynamics of PI stars. However, for SIB, additional entanglement effects are needed for a quantitative comparison with SI_2.

Acknowledgment. We are indebted to Professors W. Graessley and S. Kumar for helpful discussions and to Dr. K. L. Ngai for bringing to our attention the similarities of the data in Figures 6 and 9 with the coupling model. We also thank Professor K. Adachi for his comments on the manuscript. G.F. acknowledges the support of the Alexander von Humboldt Foundation, for a Grant (FOKOOP).

References and Notes

(1) For a review see: Bates, F. S.; Fredrickson, G. H. *Annu. Rev. Phys. Chem.* **1990**, *41*, 525.
(2) Leibler, L. *Macromolecules* **1980**, *13*, 1602.
(3) Olvera de la Cruz, M.; Sanchez, I. C. *Macromolecules* **1986**, *19*, 2501.
(4) See for example: Bates, F. S.; Rosedale, J. H.; Fredrickson, G. H. *J. Chem. Phys.* **1990**, *92*, 6255.
(5) Floudas, G.; Pakula, T.; Fischer, E. W.; Hadjichristidis, N.; Pispas, S. *Acta Polym.* **1994**, *45*, 176.
(6) Rosedale, J. H.; Bates, F. S. *Macromolecules* **1990**, *23*, 2329.
(7) Floudas, G.; Hadjichristidis, N.; Iatrou, H.; Pakula, T.; Fischer, E. W. *Macromolecules* **1994**, *27*, 7735.
(8) Stockmayer, W. H. *Pure Appl. Chem.* **1967**, *15*, 539. Baur, M. E.; Stockmayer, W. H. *J. Chem. Phys.* **1965**, *43*, 4319. Stockmayer, W. H.; Burke, J. J. *Macromolecules* **1969**, *2*, 647. Stockmayer, W. H.; Kennedy, J. W. *Macromolecules* **1975**, *8*, 351.
(9) (a) Adachi, K.; Kotaka, T. *Macromolecules* **1985**, *18*, 466. (b) Adachi, K.; Okazaki, H.; Kotaka, T. *Macromolecules* **1985**, *18*, 1687. (c) Adachi, K.; Kotaka, T. *Macromolecules* **1988**, *21*, 157. (d) Adachi, K.; Nakamoto, T.; Kotaka, T. *Macromolecules* **1989**, *22*, 3106; **1989**, *22*, 3111. (e) Watanabe, H.; Yamazaki, M.; Yoshida, H.; Adachi, K.; Kotaka, T. *Macromolecules* **1991**, *24*, 5365; **1991**, *24*, 5372. (f) Yoshida, H.; Watanabe, H.; Adachi, K.; Kotaka, T. *Macromolecules* **1991**, *24*, 2981. (g) Watanabe, H.; Urakawa, O.; Kotaka, T. *Macromolecules* **1993**, *26*, 5073. (h) Watanabe, H.; Urakawa, O.; Kotaka, T. *Macromolecules* **1994**, *27*, 3525. (i) Urakawa, O.; Adachi, K.; Kotaka, T. *Macromolecules* **1993**, *26*, 2042. (j) Yao, M.-L.; Watanabe, H.; Adachi, K.; Kotaka, T. *Macromolecules* **1991**, *24*, 2955. (k) Adachi, K.; Nishi, I.; Doi, H.; Kotaka, T. *Macromolecules* **1991**, *24*, 5843. (l) Yao, M.-L.; Watanabe, H.; Adachi, K.; Kotaka, T. *Macromolecules* **1991**, *24*, 6175.
(10) (a) Boese, D.; Kremer, F.; Fetters, L. J. *Macromolecules* **1990**, *23*, 1826. (b) Boese, D.; Kremer, F. *Macromolecules* **1990**, *23*, 829. (c) Boese, D.; Kremer, F.; Fetters, L. J. *Polymer* **1990**, *31*, 1831.
(11) Iatrou, H.; Hadjichristidis, N. *Macromolecules* **1992**, *25*, 4649.
(12) Alvarez, F. Ph.D. Thesis, Univ. del Pais Vasco, Spain, 1992. Karatasos, K.; Anastasiadis, S.; Semenov, A. N.; Fytas, G.; Pitsikalis, M.; Hadjichristidis, N. *Macromolecules* **1994**, *27*, 3543.
(13) (a) Quan, X.; Johnson, G. E.; Anderson, E. W.; Bates, F. S. *Macromolecules* **1989**, *22*, 2451. (b) Quan, X.; Johnson, G. E.; Anderson, E. W.; Lee, H. S. *Macromolecules* **1991**, *24*, 6500. (c) Floudas, G.; Fytas, G.; Brown, W. *J. Chem. Phys.* **1992**, *96*, 2164. (d) Floudas, G.; Steffen, W.; Giebel, L.; Fytas, G. *Prog. Colloid Polym. Sci.* **1993**, *91*, 124. (e) Fytas, G., et al. *Phys. Scr.* **1993**, *T49*, 237. (f) Rizos, A. K.; Fytas, G.; Roovers, J. E. L. *J. Chem. Phys.* **1992**, *97*, 6925. (g) Chung, G.-C.; Kornfield, J. A.; Smith, S. D. *Macromolecules* **1994**, *27*, 5729. (h) Alegria, A.; Colmenero, J.; Ngai, K. L.; Roland, C. M. *Macromolecules* **1994**, *27*, 4486. (i) Ngai, K. L.; Roland, C. M. *Macromolecules* **1995**, *28*, 4033. (j) Zawada, J. A.; Fuller, G. G.; Colby, R. H.; Fetters, L. J.; Roovers, J. *Macromolecules* **1994**, *27*, 6861.
(14) Hasegawa, H.; Sakurai, S.; Takenaka, M.; Hashimoto, T.; Han, C. C. *Macromolecules* **1991**, *24*, 1813.
(15) Kawahara, S.; Akiyama, S.; Ueda, A. *Polym. J. (Tokyo)* **1989**, *21*, 221.
(16) Schönhals, A. *Macromolecules* **1993**, 26, 1309.
(17) Zetsche, A.; Fischer, E. W. *Acta Polym.* **1994**, *45*, 168.
(18) (a) Pakula, T., et al., to be published. (b) Karatasos, K.; Anastasiadis, S.; Floudas, G.; Fytas, G.; Pispas, S.; Hadjichristidis, N.; Pakula, T. *Macromolecules* **1996**, *29*, 1326.
(19) Graessley, W. W. *Adv. Polym. Sci.* **1982**, *47*, 67.
(20) Rouse, P. E. *J. Chem. Phys.* **1953**, *21*, 1272.
(21) (a) Ngai, K. L.; Plazek, D. J. *J. Polym. Sci., Polym. Phys. Ed.* **1986**, *24*, 614. (b) Ngai, K. L.; Plazek, D. J.; Deo, S. S. *Macromolecules* **1987**, *20*, 3047. (c) Plazek, D. J.; Schönhals, A.; Schlosser, E. *J. Chem. Phys.* **1992**, *98*, 6488.
(22) (a) Fytas, G.; Floudas, G.; Ngai, K. L. *Macromolecules* **1990**, *23*, 1104. (b) Floudas, G.; Rizos, A.; Brown, W.; Ngai, K. L. *Macromolecules* **1994**, *27*, 2719.
(23) de Gennes, P. G. *J. Chem. Phys.* **1971**, *55*, 572.
(24) Doi, M.; Edwards, S. F. In *The Theory of Polymer Dynamics*; Clarendon: Oxford, 1986.
(25) Doi, M. *J. Polym. Sci., Polym. Phys. Ed.* **1983**, *21*, 667.
(26) Klein, J. *Macromolecules* **1978**, *11*, 852. Watanabe, H.; Tirrell, M. *Macromolecules* **1989**, *22*, 927.
(27) Stühn, B.; Stickel, F. *Macromolecules* **1992**, *25*, 5306.
(28) de Gennes, P. G. *J. Phys. (Fr.)* **1975**, *36*, 1199.
(29) Doi, M.; Kuzuu, N. *J. Polym. Sci., Polym. Lett. Ed.* **1980**, *18*, 775.
(30) Pearson, D. S.; Helfand, E. *Macromolecules* **1984**, *17*, 888.
(31) Needs, R. J.; Edwards, S. F. *Macromolecules* **1983**, *16*, 1492.
(32) Fetters, L. J.; Kiss, A. D.; Pearson, D. S.; Quack, G. F.; Vitus, F. J. *Macromolecules* **1993**, *26*, 647.
(33) Tsenoglou, C. *Polym. Prepr. (ACS, Div. Polym. Chem.)* **1987**, *28*, 185.

MA951309J